# PCCP

CrossMark
click for updates

## Study of the interface between Na-rich and Li-rich phases in a Na-inserted spinel $Li_4Ti_5O_{12}$ crystal for an electrode of a sodium-ion battery†

Mitsunori Kitta,* Riki Kataoka and Masanori Kohyama

Spinel lithium titanate (LTO; $Li_4Ti_5O_{12}$) is one of the promising materials for negative electrodes of sodium-ion batteries (SIBs). The stable charge–discharge performance of SIB cells using LTO electrodes depends on the reversible Na insertion–extraction mechanism of LTO, where the spinel lattice is expanded with Na insertion, and two phases, Na-inserted LTO (Na-LTO) and Li-inserted LTO (Li-LTO) phases, are generated. These phases are confirmed using X-ray diffraction (XRD), while the mechanism of the two-phase coexistence with different lattice volumes is yet unclear. Here, we investigate the detailed morphology of the coexisting Na-LTO and Li-LTO phases using *in situ* XRD measurements and high-resolution transmission electron microscopy (TEM) observation. Na-LTO ($a$ = 8.74 Å) and Li-LTO ($a$ = 8.36 Å) phases are confirmed in both the electrochemically formed Na-inserted LTO electrode and the single-crystalline LTO thin specimen. We observed that the Na-LTO/Li-LTO interface is parallel to the (001) plane, and contains an inevitable lattice mismatch along the interface, while the expansion of the Na-LTO phase can be partially relaxed normal to the interface. We observed that the Na-LTO/Li-LTO interface has interface layers of lattice disordering with a 1–2 nm width, relaxing the lattice mismatch, as opposed to results from the previous scanning TEM observation. How the different lattice volumes at the two-phase interface are relaxed should be the key issue in investigation of the mechanism of Na insertion and extraction in LTO electrodes.

## 1. Introduction

Sodium-ion batteries (SIBs) have been widely attracting much attention as a possible candidate for the alteration of lithium-ion batteries (LIBs).[1,2] Since there are less resource limitations for Na than Li, SIBs are more suitable for large-scale applications than LIBs. Furthermore, Fe-[3,4] or Mn-based[5,6] oxide materials could be used for the positive electrodes of SIBs, which allows us to construct lower-cost batteries than LIBs. In the studies on SIBs, a lot of useful materials have been developed for positive electrodes.[7–9] For the negative electrodes, alloy-compounds[10–12] or hard-carbons[13] were examined, however a low cycle durability or Na-metal deposition under a high reaction rate prevents practical applications. Thus new negative electrode materials for SIBs with excellent performance are highly needed.

Spinel lithium titanate (LTO; $Li_4Ti_5O_{12}$) is widely known as a safe and highly stable oxide for the negative electrode

of LIBs.[14–17] Recently, LTO has been investigated as a negative electrode for SIBs.[18–20] A relatively high electrochemical potential of the Na insertion–extraction reaction in LTO at 0.9 V *vs.* $Na^+$/Na allows us to prepare a safe negative electrode without Na-metal deposition. Furthermore, we are able to prepare a LTO electrode using a less conductive additive, due to the increment of the electron conductivity during the reduction reaction,[21,22] which reduces side reactions, prevents irreversible capacity loss, and enhances the safety performance.

Recently, we examined the properties of a carbon-free LTO electrode, as a negative electrode for SIBs, and showed that a 2V-class SIB with the same cell voltage as practical LIBs could be designed using a $LTO/NaFeO_2$ full-cell configuration.[23] We also investigated the poor rate properties of a LTO electrode with Na insertion and extraction, which were revealed to be caused by less $Na^+$ conduction in the LTO crystal than $Li^+$ conduction. Poor rate properties of Na insertion were also reported in ref. 20 and 24 and it is significantly important to settle this issue so that LTO electrodes can be used in practical SIBs. Therefore, first of all, investigation of the Na diffusion and local structural evolution during Na insertion into the LTO crystal is highly needed.

*Research Institute of Electrochemical Energy, Department of Energy and Environment, National Institute of Advanced Industrial Science and Technology (AIST), 1-8-31, Midorigaoka, Ikeda, Osaka 563-8577, Japan.*
*E-mail: m-kitta@aist.go.jp*

The bulk mechanism of Na insertion in LTO has been mainly investigated using X-ray diffraction (XRD) studies,[18–20] and the LTO diffraction peaks were observed to be divided during the Na-insertion process, suggesting a two-phase generation of Na-rich LTO (Na-LTO) and Li-rich LTO (Li-LTO; $Li_7Ti_5O_{12}$). These two phases with different lattice volumes are formed within the LTO bulk crystal, and should grow *via* mass transport through the two-phase interfaces as discussed in ref. 19. It has been considered that Na insertion induces the generation of Na-LTO as $(Na_6)^{16c}(LiTi_5)^{16d}O_{12}$ from LTO as $(Li_3)^{8a}(LiTi_5)^{16d}O_{12}$ with substantial lattice expansion due to the larger ionic radius of $Na^+$, and this successively generates Li-LTO as $(Li_6)^{16c}(LiTi_5)^{16d}O_{12}$ by pushing Li ions into the surrounding LTO within the common lattice network of $(LiTi_5)^{16d}O_{12}$, where the symbols '8a', '16c' and '16d' indicate cationic sites in a cubic spinel structure of the space group $Fd\bar{3}m$. Note that the growth of a Na-LTO phase should be attained *via* the migration of a Na-LTO/Li-LTO two-phase interface toward the Li-LTO side. The Na-LTO phase should be initially formed at the particle surface, and Na diffusion occurs through the Na-LTO phase due to the larger lattice volume. Thus Na ions are supplied from the particle surface to the two-phase interface, across which the phase conversion proceeds. Therefore, investigating the structure of Na-LTO/Li-LTO two-phase interfaces in the LTO bulk crystal is essential to understand the mechanism of phase growth and $Na^+$ diffusion. Sun *et al.* studied the structure of these two-phase interfaces using scanning transmission electron microscopy (STEM),[19] and reported that the interface between the two phases has no lattice mismatch or dislocations at the atomic level. However, the different lattice volumes of the Na-LTO and Li-LTO phases should induce some lattice distortion or dislocations at the two-phase interface. Generally, STEM imaging inevitably includes image distortion from specimen drift, or suffers from crystal-structural deterioration by electron beam damage during scanning.[25,26] Thus it is hard to discuss the detailed structure of the inter-phase interface only by using STEM imaging. By contrast, TEM imaging does not suffer from such artifacts, and should provide more reliable information on the lattice structure of the two-phase interface.

In this work, we investigate the growth of the two phases during electrochemical Na insertion into LTO electrodes using an *in situ* XRD technique, and observe the detailed morphology of coexisting Na-LTO and Li-LTO phases in a single crystalline LTO sample using TEM, which allows direct imaging of the interface lattice structure.

## 2. Experimental

### 2.1 *In situ* XRD measurements

The crystal alteration of the LTO-electrode particles during the first Na-insertion process was investigated using *in situ* XRD measurements. The electrode consists of a LTO powder (ENERMIGHT®LT-106, commercially provided by Ishihara Sangyo Kaisha, Ltd), a carbon additive (acetylene black, AB), and a binder (polyvinylidene difluoride, PVDF) at a ratio of 84 : 8 : 8 wt%. This composite powder was dispersed in *N*-methyl-pyrrolidone and mounted on 20 μm-thick Al foil. After drying the powder in a dry air-filled box ($-80$ °C d. p.) for 3 days, the electrode was punched into 1.2 cm-diameter disks with an average LTO active material loading of 8 mg per electrode. A Na-ion half-cell was constructed under dry air conditions ($-80$ °C d. p.) using an IEC R2032 coin-type cell with the LTO electrode (as the positive electrode), Na metal (as the negative electrode), and an electrolyte of 1 M $NaPF_6$ dissolved in a solvent of EC–DEC (EC/DEC = 1), where EC is ethylene carbonate and DEC is diethylcarbonate. The electrodes were separated by a micro-porous polypropylene film and a glass-filter (Advantec, GA-100). A hole was punched in the can of a CR2032-type coin cell. The Al foil current collector, on which the active material was placed, was fixed to the can with silicon grease to serve as a window for the X-ray analysis. A minimal amount of grease, sufficient to prevent the electrolyte from leaking, was applied between the cell can and the current collector, keeping the electrical contact. Other details of the construction are described elsewhere.[27] The galvanostatic Na-insertion properties of the electrochemical cells were examined for a potential window from the OCV to 0.1 V (*vs.* $Na^+/Na$) with a current density of 3 mA $(g-LTO)^{-1}$. Electrochemical Na insertion was continued at constant current without stopping during the XRD measurement cycles. A diffractometer (X'pert Pro, PAnalytical) with Mo-Kα radiation ($\lambda_1$, $\lambda_2 = 0.7093187, 0.713609$ Å) was used for the analysis. The measurement angle ($2\theta$) was adjusted from 5–50 deg, with increments of $2\theta = 0.008$ deg, over a scan time of 1 hour.

### 2.2 TEM observation

The specimen for high-resolution TEM observation was a thin $Li_4Ti_5O_{12}$ crystal prepared using a Li-vapor induction growth (Li-VIG) method,[28] where a $TiO_2(001)$ wafer with a size of $2 \times 2 \times 0.12$ mm$^3$ was thinned using an $Ar^+$ polishing system (PIPS, GATAN), and calcined with 0.3 mg of $LiOH \cdot H_2O$ in a 99.5%-$Al_2O_3$ crucible using a small electric heater at 1123 K in air for 12 hours. Then the calcined specimen was transported into a vacuum evaporation bell jar (JEE-420, JEOL), and the Na-metal evaporation source (sodium metal dispenser, SAES Getters) was attached 2–3 cm above the specimen. The jar was evacuated under vacuum until the inner pressure reached $5 \times 10^{-5}$ Pa. Then Na-metal coating was performed by heating the evaporation source electrically with conditions of 6.0 A, 2.1 V and 1 min. The total amount of Na deposited on the specimen was about $1.54 \times 10^{-8}$ mol, which corresponds to 0.41 μAh of a small electrochemical reaction. The Na-metal coated specimen was stored at $5 \times 10^{-5}$ Pa for 28 hours so as to proceed with the Na-insertion reaction and phase relaxation. The color of the specimen turned black after the reaction, due to the reduction of $Ti^{4+}$ during the Na-insertion reaction (see ESI,† Fig. S1). Then the sample was observed using FE-TEM (JEM-3000F, JEOL) at 200 kV of acceleration voltage. The collection and analysis of the TEM data were performed using a slow-scan CCD camera (Orius SC-200, GATAN) and Digital Micrograph Software (GMS 2.11, GATAN).

This journal is © the Owner Societies 2016

*Phys. Chem. Chem. Phys.*, 2016, **18**, 19888–19893 | 19889

# 3. Results and discussion

## 3.1 *In situ* XRD measurements

Fig. 1(a) shows time-sequential XRD spectra of the LTO electrode during the Na-insertion reaction. Sharp diffraction lines corresponding to 111, 311, 400, and 440 planes of the spinel $Li_4Ti_5O_{12}$ crystal ($Fd\bar{3}m$) were clearly observed for the pristine state. These diffraction lines were also observed after the Na insertion without peak shifts. These unshifted peaks can be assigned to unreacted LTO ($Li_4Ti_5O_{12}$) or Li-inserted LTO (Li-LTO; $Li_7Ti_5O_{12}$) phases. Note that the lattice-volume difference is negligible between LTO and Li-LTO.[15] According to the voltage profile of Na insertion (see ESI,† Fig. S2), the capacity was estimated to be about 160–170 mA h g$^{-1}$, after extracting the effect of side reactions of the carbon additives. This is almost the same as the theoretical capacity of LTO. Thus these unshifted peaks should be assigned to the Li-LTO phase.

Shifted peaks appeared at each lower-angle side of the unshifted peaks during the Na insertion, as indicated by black arrows in Fig. 1(a). These peaks can be assigned to a cubic spinel structure of $Fd\bar{3}m$ with a larger lattice volume than the Li-LTO phase, suggesting the growth of a Na-LTO phase.[18–20] During the Na insertion, the peak positions of the Na-LTO phase were not changed, while the intensity increased, meaning that the Na-LTO phase grows into a definite phase with a constant lattice volume from the initial stage of the Na insertion. The coexistence of the Li-LTO and Na-LTO phases seems to be similar to the two-phase coexistence in $LiFePO_4$.[29] XRD spectra from before and after the Na insertion are shown in Fig. 1(b). Black solid lines indicate the peak positions of LTO and Li-LTO, simulated with $a$ = 8.36 Å, and yellow solid lines indicate the peak positions of Na-LTO, simulated with $a$ = 8.74 Å. This lattice constant for the Na-LTO phase is consistent with that of a

previous study,[19] and the lattice volume is larger, by about 14%, than that of the Li-LTO phase. The present lattice-volume difference is significantly large, compared to the difference of 7% in a typical two-phase system of $LiFePO_4$ and $FePO_4$.[29] Therefore, there should exist a mechanism to relax the large volume change between the Na-LTO and Li-LTO phases generated in the LTO crystal, which should be revealed by microscopy analysis.

## 3.2 HR-TEM observation

To understand the coexistence features of the Li-LTO and Na-LTO phases in the LTO crystal, we performed a TEM observation of a Na-inserted LTO crystal sample as detailed in Section 2.2. Fig. 2(a) shows the low-magnification TEM image of the specimen. Some characteristic contrasts, different from the bulk region, can be seen in the surface region of the thin specimen, indicating crystal-structure changes due to the Na insertion in the surface region. In the high-magnification TEM image shown in Fig. 2(b), clear lattice fringes can be seen in both the surface and bulk regions, indicating that the Na insertion basically induces crystal-structure change or the generation of a new crystal phase, instead of deterioration of the crystal or amorphization. The 2D fast Fourier transform (FFT) pattern of Fig. 2(b) is shown in Fig. 2(c). The FFT shows clear spots corresponding to the spinel ⟨1-10⟩ diffraction pattern, indicating that the crystals in both the surface and bulk regions have cubic spinel structures of $Fd\bar{3}m$. However, each bright spot appears to be doubled, as clearly seen in the higher frequency (outer) region in the FFT pattern, which means there are different lattice volumes of the crystals in the surface and bulk regions in Fig. 2(b). For the bright spot positions of the FFT pattern indexed as 00-4, 11-5, 22-4 and 33-3, the smaller and larger inter-plane distances, calculated from each double spot and indicated by arrows, are shown in green and purple, respectively. The estimated lattice constant was $a$ = 8.36 Å for the spots with green arrows, and $a$ = 8.72 Å for the spots with purple arrows. These values are almost the same as those from the XRD analysis shown in Fig. 1(b). In this way, it can be said that the TEM specimen contains both Li-LTO and Na-LTO phases, similar to those in the XRD sample.

Fig. 3(a) shows a two-phase distribution image of Li-LTO (green) and Na-LTO (red), obtained by inverse-FFT analysis for the indexed bright spots in Fig. 2(c) indicated by green and purple arrows, respectively. This image was superimposed on the TEM image of Fig. 2(b). It is clear that the two phases exist separately in the LTO crystal. The Na-LTO phase exists in the surface region, suggesting that the Na-LTO phase would grow from the surface to the inner bulk region. Even thin Na-LTO layers near the surface seem to have a crystal structure similar to that in the LTO electrode from the electrochemical Na insertion, supporting the view that the Na-LTO phase formed in the initial Na-insertion stage does not change during the whole process (Fig. 1(a)). As the amount of deposited Na metal was small at the thin edge region of the specimen, the thickness of the Na-LTO phase was at most around 20–30 nm.

As indicated by blue arrows in Fig. 3(a), the Li-LTO/Na-LTO interface is formed parallel to the ⟨110⟩ direction and perpendicular
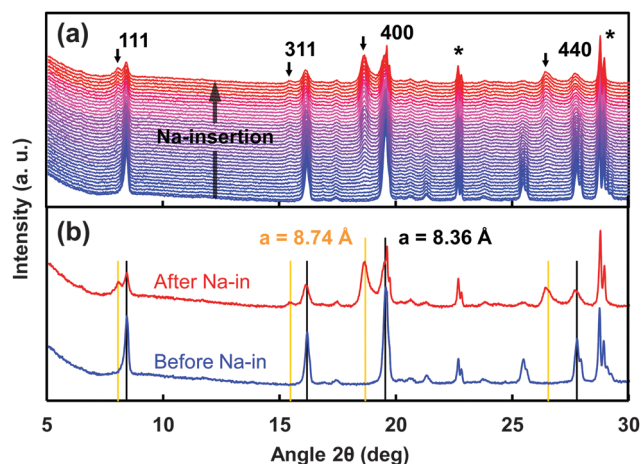


**Fig. 1** *In situ* XRD measurements of a LTO ($Li_4Ti_5O_{12}$) electrode during the Na-insertion process. (a) Time-sequential XRD spectra before (blue) and after (red) the Na insertion. Black arrows indicate the peak positions of a Na–LTO phase. Peaks assigned to the Al of the current collector are indicated by asterisks. (b) Comparison of the spectra before and after the Na insertion. Diffraction positions simulated with spinel structures of $a$ = 8.74 and $a$ = 8.36 Å are shown with yellow and black solid lines, respectively.

19890 | *Phys. Chem. Chem. Phys.*, 2016, **18**, 19888–19893

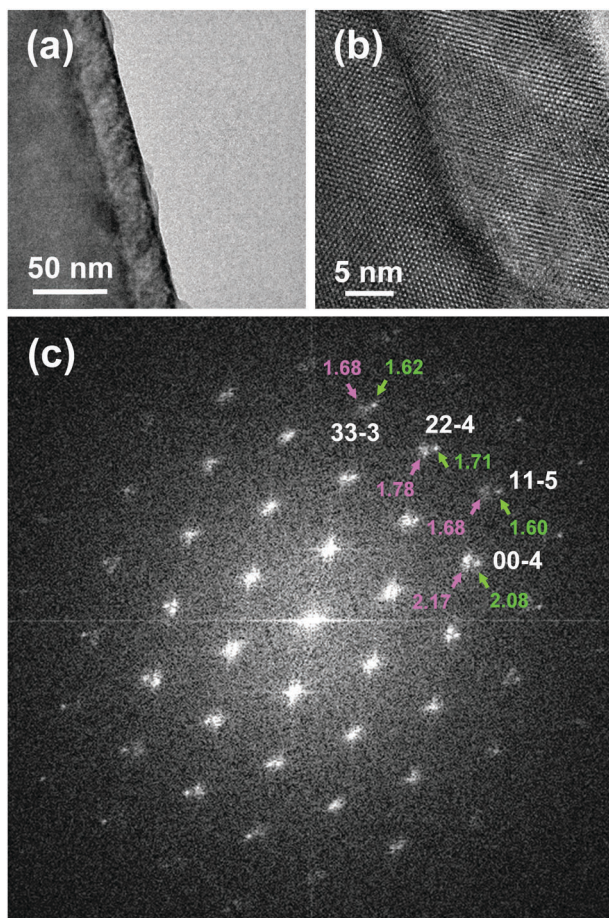This journal is © the Owner Societies 2016

Fig. 2 TEM observation of a Na-inserted LTO thin specimen. (a) Low-magnification image, observed from the spinel ⟨1-10⟩ direction. Layered contrasts can be seen near the surface region. (b) High-magnification image. Clear lattice fringes are observed in both the bulk and surface regions. (c) 2D FFT image of the TEM image in (b). The pattern of bright spots shows the features of the spinel structure. Each spot appears to be doubled, indicating the presence of two phases. Smaller and larger inter-plane distances, calculated from each double spot and indicated by arrows, are shown in green and purple, respectively.



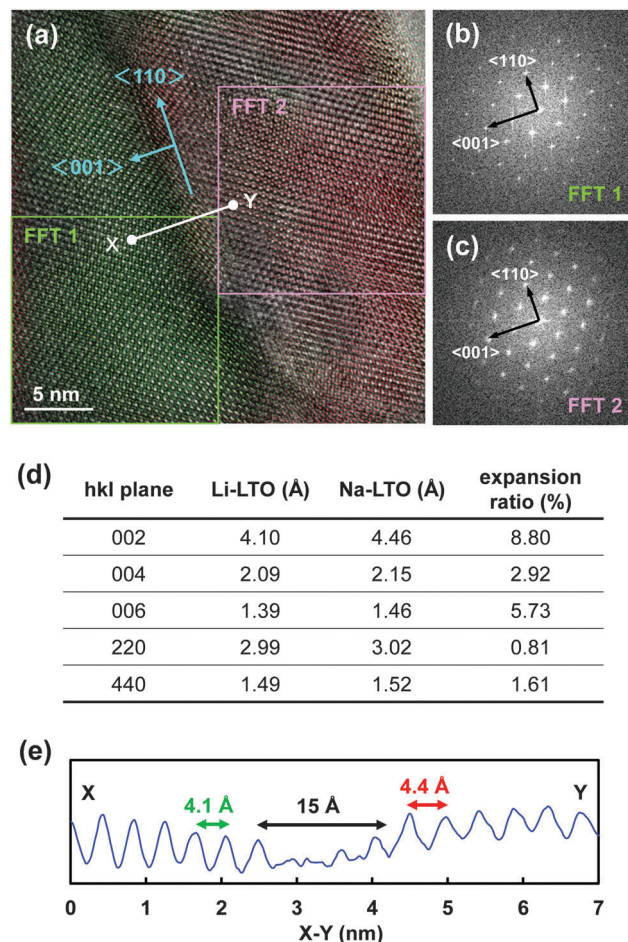| hkl plane | Li-LTO (Å) | Na-LTO (Å) | expansion ratio (%) |
|---|---|---|---|
| 002 | 4.10 | 4.46 | 8.80 |
| 004 | 2.09 | 2.15 | 2.92 |
| 006 | 1.39 | 1.46 | 5.73 |
| 220 | 2.99 | 3.02 | 0.81 |
| 440 | 1.49 | 1.52 | 1.61 |

Fig. 3 Two-phase distribution in the Na-inserted LTO specimen. (a) Distribution image reconstructed from the inverse-FFT image of bright spots in Fig. 2(c). Green and red areas are constructed from the spots indicated by green and purple arrows in Fig. 2(c), respectively. (b and c) FFT images, acquired from the areas of the TEM image enclosed by rectangles in the green and red regions in (a), respectively. (d) Inter-plane distances in the ⟨001⟩ and ⟨110⟩ directions in the Li-LTO and Na-LTO regions, obtained from the spots indicated by black arrows in (b) and (c), respectively. (e) Line profile of (001) fringes along the white X−Y line in (a).

to the ⟨001⟩ direction, in other words, it is formed on the (001) plane along the ⟨110⟩ direction. In the spinel crystal of pristine LTO, an 8a-site ion channel pathway exists through the ⟨110⟩ direction,[30,31] and fast ionic diffusion (phase growth) should be possible in this direction. Hence, the interface would be likely to form along the ⟨110⟩ direction, perpendicular to the ⟨001⟩ direction. This is similar to the Li-LTO formation in a pristine LTO crystal by Li insertion.[32] Fig. 3(b) and (c) show FFT patterns of the Li-LTO and Na-LTO regions in Fig. 3(a), respectively. The bright spots from the Na-LTO region are more obscure than those from the Li-LTO region, suggesting that the crystallinity of the Na-LTO region is lower than that of the Li-LTO region. It has been considered that Na insertion induces the generation of Na-LTO from LTO ($Li_4Ti_5O_{12}$), and successively generates Li-LTO ($Li_7Ti_5O_{12}$) by pushing Li ions into the surrounding LTO within the common lattice network.[19] Due to the larger ionic radius of $Na^+$ (102 pm) than $Li^+$ (76 pm), the Na-LTO generation in LTO

should induce much more disruption such as local distortion or defects, compared to the Li-LTO generation in LTO with a negligible lattice-volume change. This should be the reason for the lower crystallinity of the Na-LTO region. We investigated the dependence of the lattice expansion features of the Na-LTO phase on the crystal orientation. The inter-plane distances in the ⟨001⟩ and ⟨110⟩ directions in the Na-LTO region were examined, and compared with those in the Li-LTO region, as shown by black arrows in Fig. 3(b) and (c). The results are summarized in Fig. 3(d), where the lattice expansion ratios of the Na-LTO phase were calculated as follows.

$$\frac{d_{hkl(\text{Na-LTO})} - d_{hkl(\text{Li-LTO})}}{d_{hkl(\text{Li-LTO})}} \times 100 (\%)$$

The average expansion ratio is 5.8% for the ⟨001⟩ orientation, and 1.2% for the ⟨110⟩ orientation. It is clear that the expansion of the Na-LTO phase is not isotropic but anisotropic. The larger

lattice volume of Na-LTO can be partially relaxed by the lattice expansion toward the surface, namely in the direction normal to the interface, while relaxation or lattice expansion is not so easy in the direction parallel to the interface, due to the lattice connectivity between the two phases. Note that previous diffraction studies did not clarify this anisotropic relaxation of the Na-LTO phase, because of the powder samples.

There exists a lattice misfit of 1.2% in the parallel direction for the two phases on both sides of the interface. We have to consider how this misfit is relaxed in the vicinity of the interface. In Fig. 3(a), we can see a relatively dark contrast at the two-phase interface, which shows modulation of the intensity of the electron-beam diffraction by concentrated lattice strains or defects at the interface. A line profile of the (001) lattice fringes along the $X$–$Y$ segment in Fig. 3(a) is shown in Fig. 3(e). The (001) inter-plane distances in the Li-LTO and Na-LTO phases were 4.1 Å and 4.4 Å, respectively, which is consistent with a relative expansion of the Na-LTO phase of 5.8% in the $\langle 001 \rangle$ direction as explained above. The lattice fringe was obscure at the two-phase interface with about a 15 Å width, meaning that the presence of lattice disorder due to local strains, dislocations or defects relaxes the lattice misfit naturally. In a previous study,[19] these kinds of relaxation layers were not observed, while an atomically aligned connection of the two phases without any lattice disorder or dislocations was suggested. Oppositely, from the present results, we think that the existence of two-phase interfaces with relaxation layers should be general. Note that similar lattice disorder or dislocations have been confirmed for LiFePO$_4$/FePO$_4$ interfaces.[33]

Recent theoretical analysis[34] provided a typical mechanism for generation of a defective or incoherent two-phase interface from an initial coherent one, due to different lattice volumes in the case of NbC-precipitate growth in Fe. For initial small precipitates, the interface is atomically coherent, and thus the interface energy is very low. On the other hand, strains are induced over a wide extent, due to the lattice connection between the different lattice-volume phases, and the total strain energy is high. For an increasing precipitate size, the increase rate of such a bulk strain energy is much higher than for the interface area. Thus the interface structure changes from a coherent one to a defective or incoherent one so as to reduce the high total strain energy around the interface via breaking the atomic connectivity through dislocations or disordering, in spite of the much higher interface energy. The origin of the present disordered or defective structure of the Li-LTO/Na-LTO interface can be explained in a similar way.

There should generally exist structural disorder or compositional deviation at a two-phase interface due to the different lattice volumes. Even in the case of an atomically coherent interface, high strains and stresses around the interface should inevitably occur. The present case indicates a possibility that the phase conversion at the Li-LTO/Na-LTO interface, as the reaction frontier, via mass transport and an occupancy change from (Li$_6$)$^{16c}$ to (Na$_6$)$^{16c}$ across the interface, is not so simple or smooth compared to the models in ref. 19. This issue may seriously affect the diffusion and phase growth at the interface, and the rate properties of the electrode. Our recent analytical-STEM observations[35] revealed that a LTO-electrode particles

after Na insertion–extraction cycles consist of nano-domains with varied compositions of (Na$_x$Li$_{3-x}$)$^{8a}$(LiTi$_5$)$^{16d}$O$_{12}$ with $x$ values from 0 to 3, which defies the simple view in ref. 19 that phase conversion only occurs among the LTO, Na-LTO and Li-LTO phases. The observed complexity[35] may be due to the issue of two-phase interfaces having different lattice volumes. Furthermore, the Na insertion behavior with LTO was observed to be greatly dependent on the LTO-particle size.[20] This point can be understood by considering the two-phase interface with different lattice volumes, in addition to the poor diffusion of Na. As discussed in ref. 34, defective or incoherent interface structures are formed when the size of a generated phase becomes larger, due to the strain energy rapidly increasing along with the increasing phase size. Thus for smaller LTO particles, the strain energy at the coherent interface is limited, due to a limited extent of the strain, compared to larger particles with strain over a wider extent. Thus the smaller particles tend to maintain coherent interfaces in spite of substantial strain, while the larger particles tend to contain defective or incoherent interface structures, due to the much larger strain energies for coherent interfaces in the larger particles. This point may explain the remarkable dependence of the Na insertion behavior on the particle size.

Finally, we applied electrochemical impedance spectroscopy (EIS) for the cells with pristine and Na-inserted LTO electrodes so as to clarify the Na-ion behavior. As shown in Fig. S3 in the ESI,† the obtained results indicate the importance of the two-phase interface. The charge transfer resistance at the electrode/electrolyte interface is much lower for Na-inserted LTO electrodes than for pristine LTO ones, because of the generation of Na-LTO phases on the LTO particle surface regions, while some surface layers such as solid–electrolyte interphases might also be involved. The Na-ion diffusion coefficient is much larger for the Na-inserted LTO particles than the pristine LTO ones, because Na diffusion occurs more easily in the Na-LTO phases with a remarkable lattice expansion. These results support the viewpoint that growth of a Na-LTO phase is attained via migration of the two-phase interface from the Na-LTO side to the Li-LTO side, associated with Na diffusion preferentially occurring in the Na-LTO phase from the surface to the two-phase interface, where Na-ion insertion into the Li-LTO side and the phase conversion should dominate the rate properties. In this experiment, a comparison of Na-inserted cells formed using different electrochemical Na insertion rates revealed no remarkable differences, indicating no significant effects of the insertion rate at least on the properties of the generated two-phase structures, however future examination of the detailed microstructural differences including the non-equilibrium dynamic configurations would be necessary to gain deeper insight into the effect of the insertion rate.

## 4. Conclusion

In a LTO electrode, Na insertion generates both Na-LTO and Li-LTO phases, and investigation of the two-phase interface is crucial because the mass transport and phase conversion

19892 | Phys. Chem. Chem. Phys., 2016, 18, 19888–19893

This journal is © the Owner Societies 2016

across it should dominate the rate properties of the LTO electrode. In the present study, *in situ* XRD measurements confirmed that the Na-LTO phase grows as a spinel crystal of $Fd\bar{3}m$ with a constant lattice volume from the initial stage of Na insertion. TEM observation clarified that the Na-LTO phase grows from the surface region to the inner region and forms a two-phase interface with the Li-LTO phase in a Na-inserted LTO single crystal. The lattice constants of the Li-LTO and Na-LTO phases obtained from the TEM observation were 8.36 Å and 8.72 Å, respectively, which are in good agreement with those from the XRD analysis. The two-phase interface was confirmed to be located parallel to the (001) plane along the ⟨110⟩ orientation, which can be explained by faster $Na^+$ diffusion in the ⟨110⟩ direction than the ⟨001⟩ direction in the LTO spinel lattice. We observed an anisotropic expansion of the Na-LTO phase at the interface. The larger lattice volume of the Na-LTO phase can be partially relaxed normal to the interface, while there exists an inevitable lattice mismatch along the interface. A line profile of the lattice fringe clearly showed the presence of lattice disorder for about a 15 Å width at the two-phase interface, which could be caused by local strains, dislocations or defects, relaxing the lattice mismatch. This is in contrast to a previous study using STEM observation that showed no relaxation layers. The relation between the strain energy and the interface energy for a two-phase interface with different lattice volumes, depending on the size of the generated phases or the particle size, should determine the occurrence of a disordered or incoherent interface structure resulting from an initial coherent interface. In any case, how the different lattice volumes at the two-phase interface are relaxed should be the key issue in investigation of the mechanism of Na insertion and extraction in LTO electrodes.

## Acknowledgements

## References

1 K. M. Abraham, *Solid State Ionics*, 1982, **7**, 199–212.

2 L. W. Shacklette, T. R. Jew and L. Townsend, *J. Electrochem. Soc.*, 1988, **135**, 2669–2674.

3 Y. Takeda, J. Akagi, A. Edagawa, M. Inagaki and S. Naka, *Mater. Res. Bull.*, 1980, **15**, 1167–1172.

4 J. Zhao, L. Zhao, N. Dimov, S. Okada and T. Nishida, *J. Electrochem. Soc.*, 2013, **160**, A3077–A3081.

5 A. Mendiboure, C. Delmas and P. Hagenmuller, *J. Solid State Chem.*, 1985, **57**, 323–331.

6 X. Ma, H. Chen and G. Ceder, *J. Electrochem. Soc.*, 2011, **158**, A1307–A1312.

7 N. Yabuuchi, M. Kajiyama, J. Iwatate, H. Nishikawa, S. Hitomi, R. Okuyama, R. Usui, Y. Yamada and S. Komaba, *Nat. Mater.*, 2012, **11**, 512–517.

8 H. Yoshida, N. Yabuuchi and S. Komaba, *Electrochem. Commun.*, 2013, **34**, 60–63.

9 N. Yabuuchi, K. Kubota, M. Dahbi and S. Komaba, *Chem. Rev.*, 2014, **114**, 11636–11682.

10 T. R. Jow, L. W. Shacklette, M. Maxfield and D. Vernick, *J. Electrochem. Soc.*, 1987, **134**, 1730–1733.

11 L. Baggetto, P. Ganesh, R. P. Meisner, R. R. Unocic, J.-C. Jumas, C. A. Bridges and G. M. Veith, *J. Power Sources*, 2013, **234**, 48–59.

12 J. Qian, Y. Chen, L. Wu, Y. Cao, X. Ai and H. Yang, *Chem. Commun.*, 2012, **48**, 7070–7072.

13 D. A. Stevensa and J. R. Dahna, *J. Electrochem. Soc.*, 2000, **147**, 1271–1273.

14 E. Ferg, R. J. Gummow and A. de Kock, *J. Electrochem. Soc.*, 1994, **141**, L147–L150.

15 T. Ohzuku, A. Ueda and N. Yamamoto, *J. Electrochem. Soc.*, 1995, **142**, 1431–1435.

16 N. Takami, H. Inagaki, T. Kishi, Y. Harada, Y. Fujita and K. Hoshina, *J. Electrochem. Soc.*, 2009, **156**, A128–A132.

17 N. Takami, H. Inagaki, Y. Tatebayashi, H. Saruwatari, K. Honda and S. Egusa, *J. Power Sources*, 2013, **244**, 469–475.

18 L. Zhao, H.-L. Pan, Y.-S. Hu, H. Li and L.-Q. Chen, *Chin. Phys. B*, 2012, **21**, 028201.

19 Y. Sun, L. Zhao, H.-L. Pan, X. Lu, L. Gu, Y.-S. Hu, H. Li, M. Armand, Y. Ikuhara, L. Chen and X. Huang, *Nat. Commun.*, 2013, **4**, 1–10.

20 X. Yu, H.-L. Pan, W. Wan, C. Ma, J. Bai, Q. Meng, S. N. Ehrlich, Y.-S. Hu and X.-Q. Yang, *Nano Lett.*, 2013, **13**, 4721–4727.

21 M.-S. Song, A. Benayad, Y.-M. Choi and K.-S. Park, *Chem. Commun.*, 2012, **48**, 516–518.

22 C. Kim, N. S. Norberg, C. T. Alexander, R. Kostecki and J. Cabana, *Adv. Funct. Mater.*, 2013, **23**, 1214–1222.

23 M. Kitta, K. Kuratani, M. Tabuchi, R. Kataoka, T. Kiyobayashi and M. Kohyama, *Electrochemistry*, 2015, **83**, 989–992.

24 G. Hasegawa, K. Kanamori, T. Kiyomura, H. Kurata, K. Nakanishi and T. Abe, *Adv. Energy Mater.*, 2015, **5**, 1400730.

25 Y.-Q. Wang, L. Gu, Y.-G. Guo, H. Li, X.-Q. He, S. Tsukimoto, Y. Ikuhara and L.-J. Wan, *J. Am. Chem. Soc.*, 2012, **134**, 7874–7879.

26 D. Su, F. Wang, C. Ma and N. Jiang, *Nano Energy*, 2013, **2**, 343–350.

27 R. Kataoka, K. Kuratani, M. Kitta, N. Takeichi, T. Kiyobayashi and M. Tabuchi, *Electrochim. Acta*, 2015, **182**, 871–877.

28 M. Kitta, T. Akita, Y. Maeda, S. Tanaka and M. Kohyama, *Surf. Interface Anal.*, 2014, **46**, 1245–1248.

29 C. Delmas, M. Maccario, L. Croguennec, F. Lecras and F. Weill, *Nat. Mater.*, 2008, **6**, 665–671.

30 M. Wilkening, R. Amade, W. Iwaniak and P. Heitjans, *Phys. Chem. Chem. Phys.*, 2007, **9**, 1239–1246.

31 B. Ziebarth, M. Klinsmann, T. Eckl and C. Elsässer, *Phys. Rev. B: Condens. Matter Mater. Phys.*, 2014, **89**, 174301.

32 M. Kitta, T. Akita, S. Tanaka and M. Kohyama, *J. Power Sources*, 2014, **257**, 120–125.

33 G. Chen, X. Song and T. J. Richardson, *Electrochem. Solid-State Lett.*, 2006, **9**, A295–A298.

34 H. Sawada, S. Taniguchi, K. Kawakami and T. Ozaki, *Modell. Simul. Mater. Sci. Eng.*, 2013, **21**, 045012.

35 M. Kitta, K. Kuratani, M. Tabuchi, N. Takeichi, T. Akita, T. Kiyobayashi and M. Kohyama, *Electrochim. Acta*, 2014, **148**, 175–179.

This journal is © the Owner Societies 2016

*Phys. Chem. Chem. Phys.*, 2016, **18**, 19888–19893 | **19893**